Dynamic wetting of viscoelastic droplets

Yuli Wang[*]
Linné FLOW Center, Department of Mechanics, The Royal Institute of Technology, 100 44 Stockholm, Sweden and School of Energy and Power Engineering, Jiangsu University, 212013 Zhenjiang, China

Do-Quang Minh[†] and Gustav Amberg[‡]
Linné FLOW Center, Department of Mechanics, The Royal Institute of Technology, 100 44 Stockholm, Sweden
(Received 25 June 2015; revised manuscript received 11 September 2015; published 5 October 2015)

We conduct numerical experiments on spreading of viscoelastic droplets on a flat surface. Our work considers a Giesekus fluid characterized by a shear-thinning viscosity and an Oldroyd-B fluid, which is close to a Boger fluid with constant viscosity. Our results qualitatively agree with experimental observations in that both shear thinning and elasticity enhances contact line motion, and that the contact line motion of the Boger fluid obeys the Tanner-Voinov-Hoffman relation. Excluding inertia, the spreading speed shows strong dependence on rheological properties, such as the viscosity ratio between the solvent and the polymer suspension, and the polymeric relaxation time. We also discuss how elasticity can affect contact line motion. The molecular migration theory proposed in the literature is not able to explain the agreement between our simulations and experimental results.

DOI: 10.1103/PhysRevE.92.043002 PACS number(s): 47.50.Cd, 47.55.np, 47.11.Fg, 47.63.mf

I. INTRODUCTION

Wetting of non-Newtonian fluids is an important industrial process in inkjet printing, coating, cleaning, and additive manufacturing to name a few. The spreading of a non-Newtonian droplet on a horizontal surface is a benchmark problem rising from the aforementioned applications. A reduced problem, the spreading of Newtonian droplets, follows some universal rules such as the Tanner's law that describes the spreading radius as a function of time [1], and the Tanner-Voinov-Cox relation that reveals the dependence of contact line speed on dynamic contact angle [2–4], both of which are valid for the late time spreading behavior. However, for non-Newtonian fluids, studies have reported very different observations and drawn contradictory conclusions on both spreading (receding) dynamics and contact line dynamics.

Two rheological features have attracted major interest in the study of non-Newtonian wetting: the shear thinning which is commonly present in power-law fluids, and the normal stress effect that characterizes elastic fluids.

Experiments have found that the wetting kinetics of power-law, shear-thinning droplets shows strong deviation from the behavior of Newtonian droplets [5–7]. Rafaï *et al.* [6] reported that a xanthan solution spreads slightly slower than a Newtonian fluid, in terms of the spreading radius over time. Their interpretation of this observation was that the apparent contact angle is reduced by shear thinning; hence the capillary force driving the contact line becomes smaller. There is, however, evidence that proves that shear-thinning fluids spread faster than Newtonian fluids. Wei *et al.* discovered shear-thinning fluids have much weaker dependence of spreading speed on the apparent contact angle. In their experiment the shear thinning 0.15 wt % xanthan gum solution spreads much faster than the Newtonian 10P polydimethylsiloxane (PDMS) solution [8].

Research on the normal stress effect on contact line motion tells an attractive story. It is believed that Boger fluids, which show viscoelasticity without shear thinning, follow the Tanner-Voinov-Hoffman (COX) relation [9]. Han and Kim [10] further stated that the contact line motion can be enhanced by increasing polymer concentration, i.e., providing higher degree of elasticity. They suggested, with supportive proof from the experiment by Fang *et al.* [11] on DNA molecules, that the stretched polymers near the contact line may migrate away from the wall, reducing the effective viscosity in the contact region. An interesting debate rises from the discussions on wetting involved in the non-Newtonian droplet impact. In the experiment by Bergeron *et al.* [12], the droplet of dilute polyethylene oxide (PEO) solution spreads similar to Newtonian droplets, but its receding speed is dramatically reduced. More excitingly, the rebound of droplets of high impact speed is suppressed. This result has promising commercial perspectives because one can enhance the droplet deposition on a hydrophobic surface, which is an important process for the agrochemical industry. Early studies believed that the slowing down of contraction is due to the extensional viscosity contributed by the polymeric fluid [13,14]. Bartolo *et al.* pointed out later that the deceleration of contraction is caused by the normal stress difference that developed near the contact line [15]. However, Smith and Bertola [16] measured the actual receding speed and proved that given the same spreading radius, the droplet of 200-ppm PEO solution contracts as fast as the water droplet. They proposed that the slowing down is due to the stretching of polymer molecules inside a thin film beyond the droplet when the contact line sweeps over the surface. This finding is supported by Bertola [17].

Non-Newtonian rheology also influences the contact line morphology. Given a constant contact line speed, the viscous bending of the vapor-gas interface near the wall is reduced for shear-thinning fluids [18] but is enhanced by elasticity [9,19].

[*]yuli@mech.kth.se
[†]minh@mech.kth.se
[‡]gustava@mech.kth.se

We notice that in order to clarify the rheological impact on wetting, it is important to isolate the rheological effect from the combined effect from multiple factors such as viscosity ratio, inertia, gravity, etc. However, few among previous studies has considered fluids with equal static properties such as density, zero-shear viscosity, molecular weight of polymer additives, etc. In non-Newtonian droplet impact experiments, inertia usually dominates the effects created by the polymeric fluid, and thus little deviation from Newtonian behavior was observed, despite the strong extensional flow present in the spreading stage [20]. Practically, it is difficult to exclude inertia or gravity in an experiment. Numerical simulation, to this extent, is competitive since one can easily switch on or off certain physics. However, the published numerical efforts to resolve non-Newtonian wetting is very limited compared to the large number of simulations on wetting of Newtonian fluids. The existing contact line models and non-Newtonian constitutive models do not account for some physics that are discussed by experiments, e.g., depleted molecules near the wetting substrate, molecules stretched in the thin film left behind a receding contact line. Will they be able to capture the wetting behavior of non-Newtonian droplets qualitatively or even quantitatively?

In this work we numerically simulate the spreading of non-Newtonian droplets. The diffuse interface method has been used to describe the moving contact line, a viscoelastic constitutive model to present the rheology of a polymeric solution and the Stokes equations that characterize inertialess flow. We examine the influence of both viscoelasticity and shear thinning on wetting dynamics.

II. MODELS

We focus on a viscoelastic droplet made of Oldroyd-B fluid and Giesekus fluid in an axisymmetric plane, spreading on a horizontal surface, depicted in Fig. 1. We assume the surface is completely homogeneous without contact line hysteresis. The droplet is immiscible with the ambient Newtonian fluid. The interface between two phases is described by the phase field variable ϕ, where $\phi = 1$ denotes the droplet phase and $\phi = -1$ denotes the ambient fluid. The evolution of ϕ is governed by the Cahn-Hilliard equations [21]:

$$\frac{\partial \phi}{\partial t} + \nabla \cdot (\mathbf{u}\psi) = \gamma \triangle \psi, \tag{1}$$

$$\psi = -\zeta\left(\triangle\phi + \frac{\phi^3 - \phi}{\epsilon^2}\right), \tag{2}$$

where γ is the mobility parameter, ζ is the mixing energy density, ϵ is the characteristic width relating to the interfacial thickness, and the surface tension coefficient is determined as $\sigma = 2\sqrt{2}\zeta/3\epsilon$. We assume local equilibrium at the liquid-solid interface. The equilibrium contact angle can be implemented by the boundary condition for Eq. (2) [22,23]:

$$\zeta \nabla\phi \cdot \mathbf{n} + \sigma\cos(\theta_e)g'(\phi) = 0, \tag{3}$$

where $g'(\phi)$ is the derivative of the local surface energy $g(\phi) = 0.25 - 0.75\phi + 0.25\phi^3$, and $\mathbf{n}$ is the unit vector normal to the substrate. Besides, we assume that there is no mass flux from the substrate, i.e., $\mathbf{n} \cdot \nabla\psi = 0$. The flow is governed by the Stokes equations that account for momentum conservation and mass conservation of a mixed incompressible system:

$$-\nabla p + \nabla \cdot \beta\eta[\nabla\mathbf{u} + (\nabla\mathbf{u})^{\mathsf{T}}] + \nabla \cdot \boldsymbol{\tau}_d + \psi\nabla\phi = 0, \tag{4}$$

$$\nabla \cdot (\rho\mathbf{u}) = 0, \tag{5}$$

where the term $\psi\nabla\phi$ represents the surface tension force [24], and η is the mixed viscosity interpolated by $\eta_d(1+\phi)/2 + \eta_m(1-\phi)/2$. Here the subscript d denotes the droplet phase and m the ambient fluid. $\rho = \rho_d(1+\phi)/2 + \rho_m(1-\phi)/2$ is the mixed density. For simplicity, we assume the droplet fluid and ambient fluid have the same viscosity and density, i.e., $\rho_m = \rho_d = \rho, \eta_m = \eta_d = \eta$. $\beta = \beta_d(1+\phi)/2 + \beta_m(1-\phi)/2$ is the viscosity ratio of the polymer solution, and $\beta_m = 1$ for the ambient fluid. The no-slip condition $\mathbf{u} = 0$ is applied to the substrate. The term $\boldsymbol{\tau}_d$ is the polymeric stress calculated by the constitutive equations:

$$\boldsymbol{\tau}_d + \lambda\boldsymbol{\tau}_d(l) + \frac{\lambda\alpha}{\eta(1-\beta)}(\boldsymbol{\tau}_d \cdot \boldsymbol{\tau}_d) = \eta(1-\beta)[\nabla\mathbf{u} + (\nabla\mathbf{u})^{\mathsf{T}}], \tag{6}$$

where $\boldsymbol{\tau}_d(l)$ is the upper-convected time derivative of $\boldsymbol{\tau}_d$ [25], and $\eta(1-\beta)$ is the viscosity contributed by the polymer chains in the polymeric solution. λ is the polymeric relation time that reflects elasticity, interpolated by $\lambda_d(1+\phi)/2 + \lambda_m(1-\phi)/2$, and $\lambda_m = 0$ for the ambient fluid. α is a model parameter from the Giesekus model, and $\alpha = 0$ gives the Oldroyd-B model.

Scaling Eqs. (1)–(6) by the capillary speed $U_0 = \sigma/\eta$, the initial droplet radius R, the capillary time scale $R\eta/\sigma$, and the reference stress σ/R, we obtain the following nondimensional parameters: the Pèclet number $\mathrm{Pe} = 2\sqrt{2}U_0\epsilon R/3\sigma\gamma$, expressing the ratio between advection and diffusion of the interface; the Cahn number $\mathrm{Cn} = \epsilon/R$ that expresses the ratio between the interfacial thickness and the droplet initial radius; the capillary number $\mathrm{Ca} = \eta U_0/\sigma$ that controls the relative

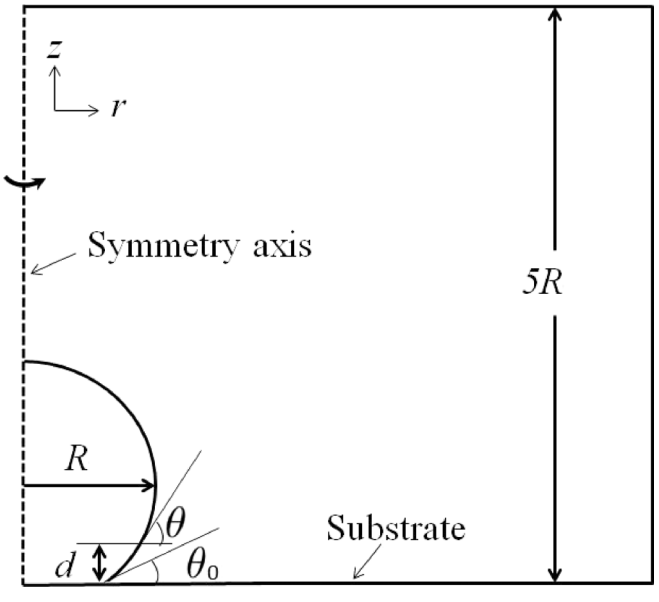

FIG. 1. Computational domain and initialization of the droplet.

importance of viscosity over capillarity, $\mathrm{Ca} = 1$ throughout our simulation; and the Weissenberg number $\mathrm{Wi} = \lambda U_0/R$ that denotes the degree of elasticity. Cn, Pe are phase field parameters that influence interface width and bulk diffusion. Following the guidelines for picking proper values for them in the literature [19,26], we fix $\mathrm{Pe} = 100$ and $\mathrm{Cn} = 0.005$ to maintain a stable sharp interface in the simulation. In the following, we use nondimensional quantities. Note that we use a reference time of $10R\eta/\sigma$ in the following figures, considering it will give a more clear vision of our data.

III. NUMERICAL METHODS

Equations (1) and (6) are discretized in a finite element space by the standard Galerkin method. We apply the forward Euler method to all the time derivatives above. The resulting system in a weak formulation is solved by a segregated routine. First, the Cahn-Hilliard group, i.e., coupled Eqs. (1) and (2), is solved by the Newton method. Second, the constitutive equations, i.e., Eq. (6), is solved by the Newton method. In each Newton iteration we applied the direct solver MUMPS [27,28]. Thereafter the augmented Stokes system, i.e., coupled Eqs. (4) and (5), is also solved by MUMPS directly. The DEVSS-G scheme is adopted to enhance the numerical stability of solving the constitutive equation [29].

An adaptive mesh refinement routine is applied in our simulation, which provides spatial resolution around the droplet-ambience interface and helps to resolve the high polymeric stress gradient in the contact region.

The above numerical system is implemented using the finite element toolbox FEMLEGO [30]. FEMLEGO allows customized setup of weak formation, initial and boundary conditions, and solver types in a single MAPLE worksheet.

IV. RESULTS AND DISCUSSION

A. Droplet spreading

The spreading of a droplet can be considered as divided into three regimes: the initial short time spreading when the droplet starts to touch the substrate; the inertial or the viscous wetting in which the bulk droplet spreads onto the surface, characterized by the Reynolds number Re showing the relative dominance between inertia and viscosity (in this simulation we focus on the viscous spreading and we neglect inertia, i.e., $\mathrm{Re} = U_0 R/\eta \ll 0.1$); and the late time spreading when the contact angle is very near to the equilibrium angle. The dissipative mechanism of the initial spreading of a viscous droplet is still not clear [31,32]; therefore we skip this stage in our simulation and focus on the viscous wetting and late time dynamics to better compare with the existing studies. Droplets are initialized such that they are already attached to the horizontal surface, with an initial contact angle $\theta_0 = 120^\circ$ (see Fig. 1). The prescribed boundary condition in Eq. (3) sets the equilibrium contact angle to be 43°. The discrepancy between the apparent contact angle θ and the microscopic contact angle creates a curved interface in the contact region [see Fig. 2(a)]. The resulting capillary force driving the contact line moves to the right and droplets start spreading from the initial position to reach their equilibrium state in which $\theta_e = \theta$.

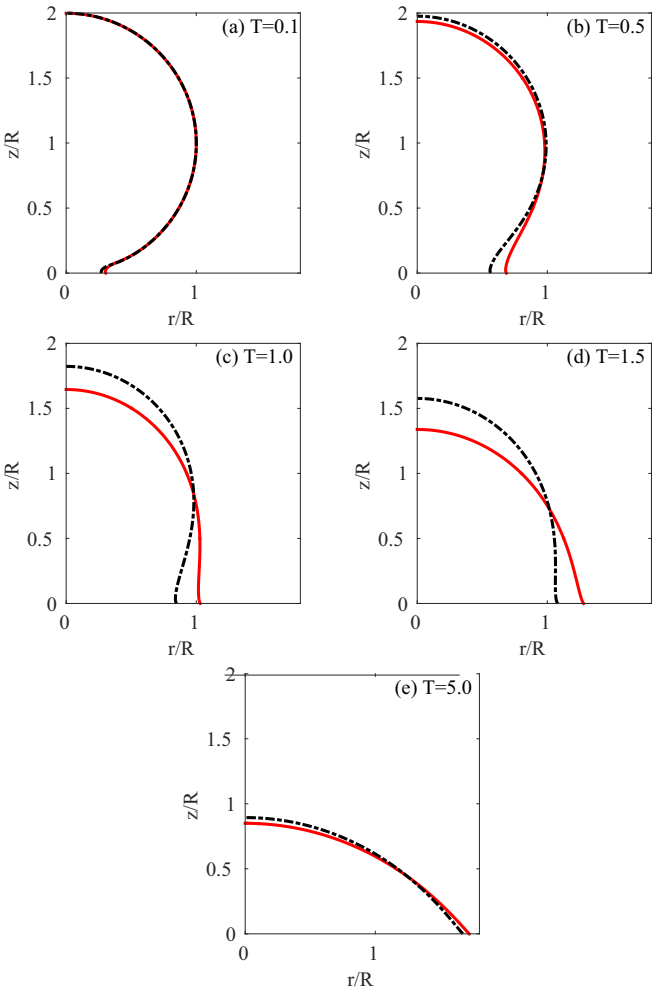

FIG. 2. (Color online) Spontaneous plot of droplet profiles. $\theta_e = 43^\circ$, droplet profiles are plotted as contours of $\phi = 0$, the black dash-dot curve represents the Newtonian droplet, and the red solid curve represents the Giesekus droplet of $\mathrm{Wi} = 5, \beta = 0.2$.

A clear observation from Fig. 2 is that the Giesekus droplet spreads faster than the Newtonian droplet throughout the process, starting from the same initial displacement. The Giesekus droplet starts to overtake the Newtonian droplet already at the beginning of spreading, with its contact line a bit ahead of the Newtonian contact line, as seen in Fig. 2(a). When the bulk of the Giesekus droplet accelerates, at $T = 0.5$ the two droplets show evident discrepancy upon displacement, shown in Fig. 2(b). The gap between contact lines increases until it reaches the maximum at around $T = 1.5$ when the Newtonian droplet has an apparent contact angle around 90°. Thereafter the Newtonian droplet starts to catch up with the Giesekus droplet when the Giesekus droplet decelerates as it is approaching the equilibrium contact angle, and the gap between the contact lines closes up. The above observation agrees with several experimental observations on wetting of shear-thinning fluids [5–7]. In the presented results droplets always have identical final spreading radius, while in the droplet impact experiments the maximum spreading radius depends on inertia through the impact speed. In the viscous spreading regime studied here, the non-Newtonian effect is

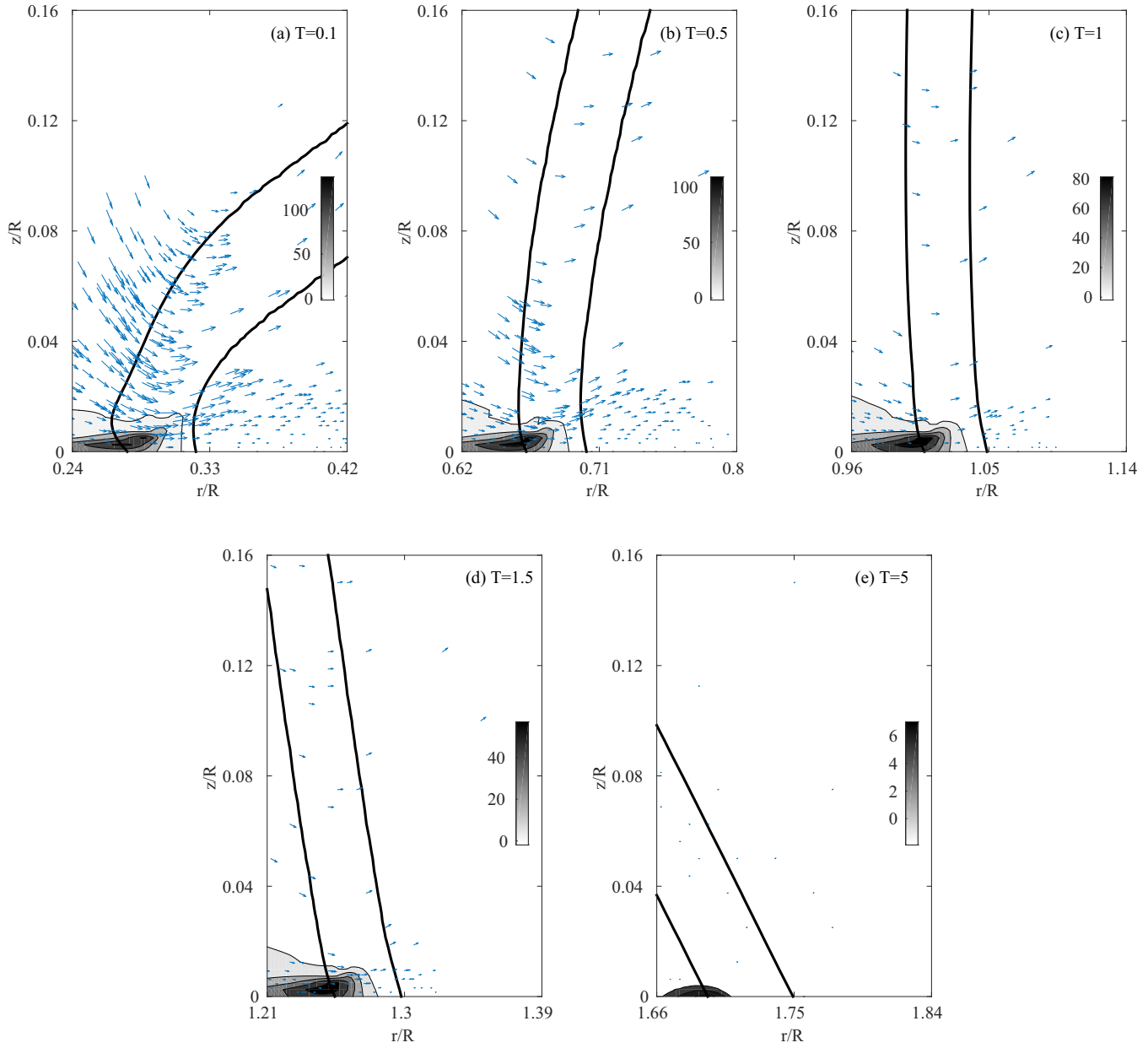

FIG. 3. (Color online) $\theta_e = 43^\circ$, Giesekus droplet with $\mathrm{Wi} = 5, \beta = 0.2$: contours plot the normalized polymeric first normal stress difference $10(\tau_{prr} - \tau_{pzz})/(\sigma/R)$, the two solid lines correspond to $\phi = -0.9$ and $\phi = 0.9$, respectively, and vectors are scaled by velocity magnitude.

quite visible throughout the spreading process, while during droplet impact, inertia always overcomes non-Newtonian effects and viscoelastic droplets spread like Newtonian droplets [15,33]. However, it is not clear whether shear thinning or viscoelasticity causes faster spreading since the Giesekus fluid possesses both features.

The first normal stress difference $\tau_{prr} - \tau_{pzz}$ has been extracted to examine the viscoelasticity, and its distribution in the vicinity of the contact line is plotted in Fig. 3. The polymeric stress concentrates in a thin layer near the wall, in accordance with the literature [19,34]. Initially the contact line is subject to great forcing because the contact angle is far away from equilibrium. This generates the largest advancing velocity along the wall, shown in Fig. 3(a), and consequently, the largest velocity gradient along the wall. Due to the acceleration of the contact line, the polymer molecules around the contact region are stretched along the advancing direction. Given the no-slip condition at the wall, this implies the largest shear rate $\partial u_r/\partial z$, where u_r is the r component of $\mathbf{u}$. The normal stress difference increases accordingly, since it has a quadratic relation with shear rate $\tau_{prr} - \tau_{pzz} \propto (\partial u_r/\partial z)^2$. Therefore we observe the maximum value of normal stress in the beginning of spreading. While spreading, the curvature of the contact line decreases, the driving force is weaker, and the advancing velocity decreases accordingly. Polymer chains in the contact region relax so the first normal stress difference goes down [see Figs. 3(b)–3(d)]. In the late time spreading in the contact line relaxes towards the equilibrium

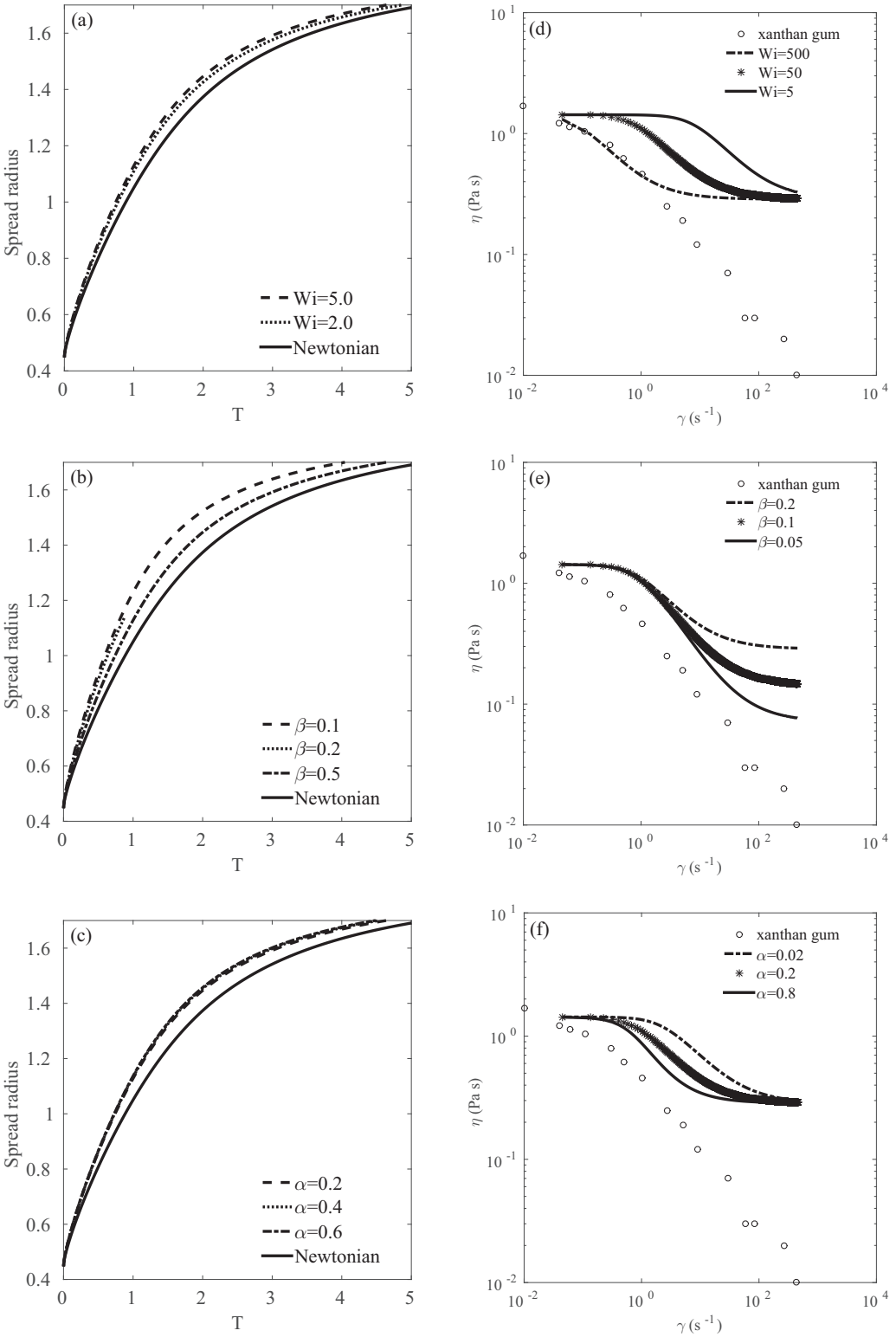

FIG. 4. Dependence of spreading radius on model parameters, $\theta = 43^\circ$. The left column: (a) Spreading radius for different Wi, α, and β are fixed to be 0.2 and 0.5, respectively. (b) Spreading radius for different β, Wi, and α are fixed to be 5.0 and 0.2, respectively. (c) Spreading radius for different α, Wi, and β are fixed to be 5.0 and 0.5, respectively. The right column shows calibration of η vs γ of the Giesekus model against 15 wt% xanthan gum under steady shear, and circles present measured data [18]. (d) $\beta = 0.2$, $\alpha = 0.2$. (e) Wi $= 50$, $\alpha = 0.2$. (f) Wi $= 50$, $\beta = 0.2$.

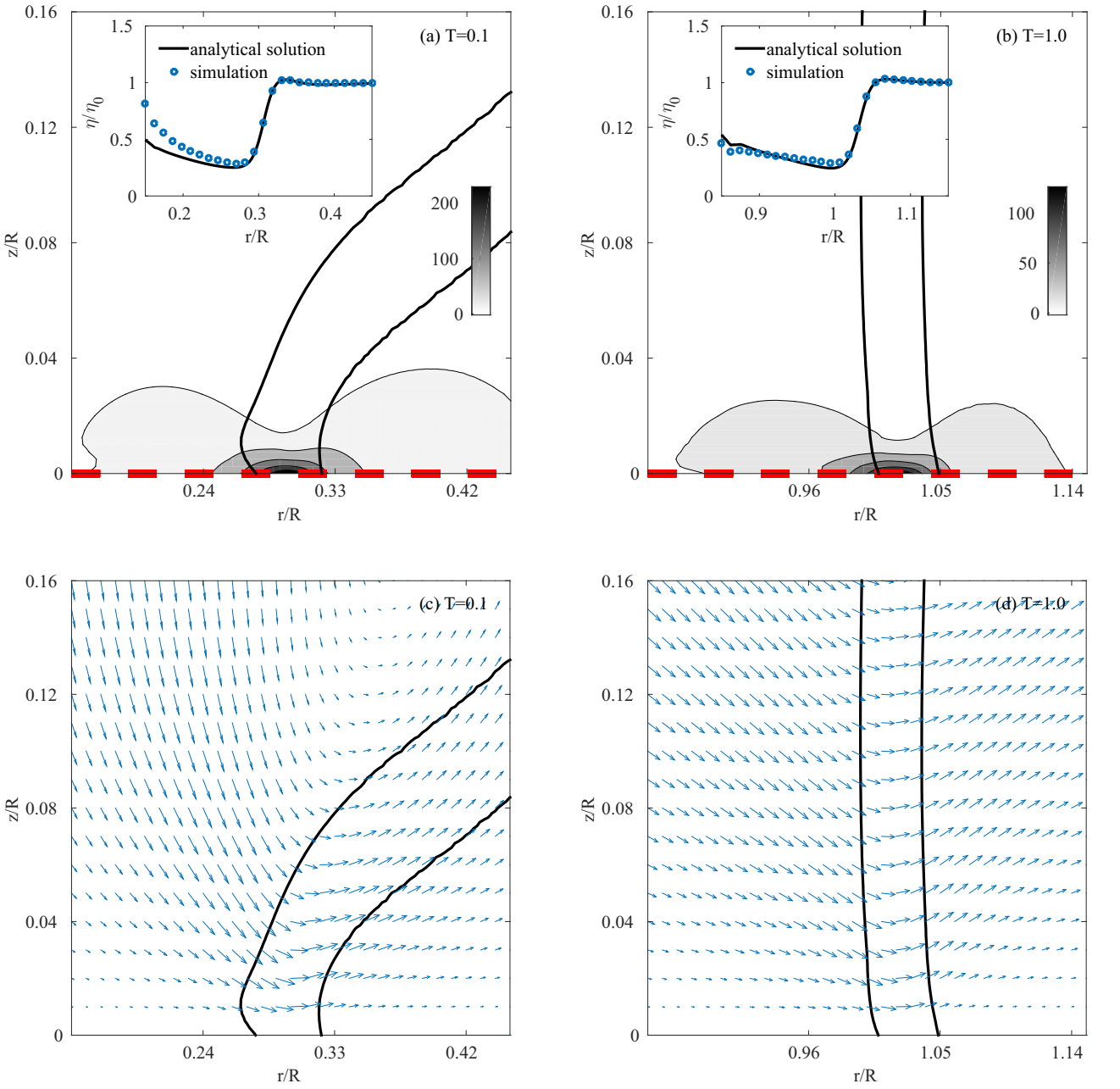

FIG. 5. (Color online) $\theta_e = 43^\circ$,Wi $= 5.0, \beta = 0.2, \alpha = 0.2$. Contours plot shear rate $\dot{\gamma}$, and the small chart shows the shear viscosity η/η_0 along the red dashed line, computed by both analytical expression and $\boldsymbol{\tau}_p/\dot{\gamma}$. The solid lines are the contour lines of $\phi = -0.9$ (right) and $\phi = 0.9$ (left). The interface is advancing from left to right. Vectors show the flow field around the contact line.

and finally becomes static, the interface becomes straight, i.e., θ is consistent with θ_e, the stress region shrinks to a tiny area, and the value of stress is nearly zero, shown in Fig. 3(e). To summarize the observation above, the shear rate near the contact line during spreading is the key factor that introduces the viscoelastic effect.

B. Effects of model parameters

The properties of Giesekus fluids represented by Eq. (6) are adjusted by Wi, β, and α. Increasing Wi or β or both enhances fluid elasticity, while α sets the weight of the quadratic nonlinearity and is a regulation parameter that sets the plateau of the growth of $\boldsymbol{\tau}_d$. Both Wi and α have a mild impact on the spreading [see Figs. 4(a) and 4(c)]. The enhanced polymer relaxation which normally results in a larger extensional viscosity does not decelerate the spread but instead speed up the contact motion. Variation of α introduces an almost invisible difference on the spreading radius over time. By reducing the weight of solvent viscosity among the total viscosity, we observe a growth of the spreading radius [see Fig. 4(b)].

Figures 4(d)–4(f) show the dependence of shear viscosity on Wi, β, and α under a flow geometry of steady shear. One can see that the Giesekus fluid remains Newtonian in a certain range of shear rate. The critical shear rate where

shear thinning starts to take place depends on Wi and α. Increasing Wi or α can trigger shear thinning with a smaller critical shear rate [see Figs. 4(d) and 4(f)]. The minimum shear viscosity after shear thinning does not depend on Wi or α, as all curves in Figs. 4(d) and 4(f) eventually converge to the same value of shear viscosity, given the identical β. On the other hand, fixing Wi and α gives identical critical shear rate, while the lowest limit of shear viscosity is decided by β, i.e., smaller β gives smaller minimum shear viscosity [see Fig. 4(e)]. The above observations explain to some extent the reason why the spreading is enhanced by larger Wi and α, as the shear thinning happens earlier during droplet spreading and reduces resistance at the contact line. Besides, since β decides the actual viscosity in the shear-thinning region, it is straightforward to understand that the droplet of $\beta = 0.1$ experiences the least drag force during spreading and therefore spreads faster, as shown in Fig. 4(b).

To verify the observations above, we zoom at in the contact region and examine the shear viscosity there. Assuming the parameters presented here can make the Giesekus fluid shear-thinning dominant, and the spreading is affected by the actual shear viscosity in the contact region. If one looks close into the contact region of a shear-thinning fluid, the shear-thinning region only occupies a thin layer covering the wall while the rest of the contact region remains Newtonian [18]. The flow near the contact line is close to simple shear; see snapshots of the velocity field in Fig. 3. The actual shear viscosity can be estimated by $\eta/\eta_0 = \tau_{rz}/\dot{\gamma}$, where τ_{rz} is the shear component of the normalized polymeric stress tensor $\boldsymbol{\tau}_d R/\eta U_0$, and $\dot{\gamma}$ is the normalized shear rate defined by $\partial u_r R/\partial z U_0$. The presented Giesekus model has an analytical solution for viscosity in simple shear flow geometry. For our two-phase system the shear viscosity of Giesekus fluid as a function of shear rate is given by [25,35]

$$\eta/\eta_0 = \beta + (1-\beta)\frac{(1-\Pi)^2}{1+(1-2\alpha)\Pi}, \tag{7}$$

where $\Pi = \frac{1-\chi}{1+(1-2\alpha)\chi}, \chi^2 = \frac{[1+16\alpha(1-\alpha)\mathrm{Wi}]^{0.5}-1}{8\alpha(1-\alpha)(\mathrm{Wi}\dot{\gamma})^2}$. Extracting $\dot{\gamma}$ from the simulation and subtracting it into Eq. (7), the viscosity from the analytical function is obtained. As shown in Fig. 5, it is clear that the shear viscosity continuously decreases towards the interface due to the shear thinning, then increases sharply within the interface, and is finally constant in the Newtonian fluid ahead of the interface. The shear rate concentrates in the interfacial region which spans around two interface thickness in the radial direction. Shear-thinning effects are restricted in this area. In early stage spreading, the bending of the interface causes a downward flow in the droplet phase and upward flow outside the droplet, shown in Fig. 5(c). Due to the mismatch of flow field, the analytical result based on simple shear flow underestimates the actual shear viscosity [see Fig. 5(a)]. During viscous spreading, shown in Fig. 5(b), the interface is less curved, the flow geometry in the shear-thinning region is more likely steady shear [see Fig. 5(d)], and therefore the calculated viscosity fits the analytical result well. The implementation of the Giesekus model correctly predicts the shear viscosity in the shear-thinning region near the contact line. The shear rate is smaller compared to the early stage as the advancing of the contact line becomes mild. We can conclude that the underlying mechanism that makes the Giesekus droplet faster than the Newtonian droplet is the rheological property of Giesekus fluid under simple shear.

TABLE I. Measurement of $1/k$ in Fig. 6 and the literature.

Case	Wi	α	$1/k$
N/N	0	0	0.5054
O/N	5	0	0.8251
O/N	45	0	1.041
O/N	450	0	1.0842
G/N	5	0.2	1.0797
G/N	450	0.2	1.0799
4.2 M [10]	12.73	0	0.3208
500k [10]	1.5818	0	0.1058

Considering that the onset of shear thinning depends on the shear rate around the contact line, it is rational to expect that the spreading speed converges in the late spreading as the viscosity of Giesekus fluid recovers to the Newtonian viscosity, given the small shear rate, and then the droplet shall spread as fast as the Newtonian droplet; however, this is not the case in our simulation, and we visit this problem in the next section.

C. Contact line speed

The late time spreading dynamics of Newtonian fluids are characterized by the linear dependence of Ca on θ, with $1/k$ indicating the speed of spreading, shown in Table I, where k is the slope depicted in Fig. 6(b). Here we measured the apparent contact angle at a fixed distance of $d >$ Cn, where the measurement does not depend on d (see Fig. 1). In Fig. 6, for several viscoelastic fluids and the Newtonian fluid of the same zero shear viscosity, we measure the contact line speed as a function of dynamic contact angle. Note, here we use the local capillary number defined by $\mathrm{Ca} = U\eta/\sigma$ to represent the contact line speed, where U is the spontaneous advancing velocity of the contact line in the simulation. The corresponding apparent angle is recorded simultaneously. It is clear that both the Oldroyd-B fluid and the Giesekus fluid spread faster than their Newtonian counterpart, even when they are near the equilibrium state, and they all hold a linear relation between Ca and θ. For the shear-thinning-dominated Giesekus droplet, the contact line motion shows no dependence on elasticity since the variation of Wi does not affect the slope k. The slope is only decided by the viscosity of the solvent fluid. For the Oldroyd-B droplet, the contact line motion is enhanced by the increase of Wi. The droplet with small polymer relaxation ($\mathrm{Wi} = 5.0$) spreads as fast as the Newtonian droplet. $1/k$ increases with Wi, but its growth is limited by a maximum value which coincides with that of the Giesekus fluid.

Our observation on the Oldroyd-B fluid agrees with the results reported by Han and Kim, who conducted measurement on Boger droplet spreading on a flat surface [10]. They reported that for the polyisobutylene (PIB) Boger fluid, which is close to the Oldroyd-B fluid, Ca varies linearly with θ. The spreading speed increases with polymer concentration, or relaxation time, for solution with high molecular weight. More

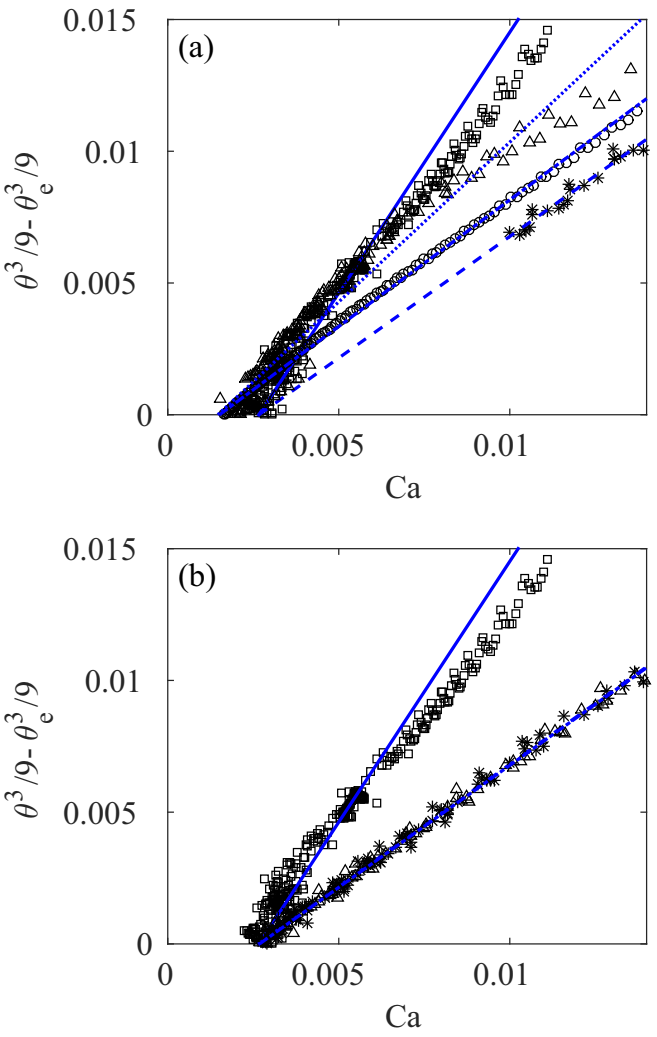

FIG. 6. (Color online) Ca vs θ of the Newtonian droplet (squares) and viscoelastic droplets of different Wi, triangles: Wi = 5, circles: Wi = 45, stars: Wi = 450. Lines of different styles represent linear fits of the data of each case. Fixed parameters are $\beta = 0.1, \theta = 90^\circ, \alpha = 0.1$. (a) Comparisons between the Newtonian droplet and Oldroyd-B droplets, and (b) comparison between the Newtonian droplet and Giesekus droplets ($\alpha = 0.2$).

specifically, for their PIB/PB solution with higher molecular weight of 4.2 M, k continuously increases with polymer concentration from 620 to 2500 ppm. Given their measurement of physical properties, this corresponds to Wi = 2–13 using our scaling. While for the low-molecular-weight solution of 500k, k seems not to be sensitive to polymer concentration and the solution acts like a Newtonian fluid. If we examine Wi of the 500k solution, the concentration shifting from 3500 to 14 000 ppm results only in a variation of Wi from 0.58 to 2.9, far below the range where one can observe an evident viscoelastic effect in our simulation, say, beyond Wi = 5. This explains why elasticity only takes effect in their high-molecular-weight solution and the 4.2-M solution spreads faster (see in Table I).

If one revisits the molecule immigration theory explained by Han and Kim [10], Fang *et al.* [11], and Ma and Graham [36], saying the polymer molecules subject to shear will move away from the near wall layer and this motion is enhanced by elasticity, one can imagine that given a certain degree of elasticity all molecules will move out of the layer, leaving the effective viscosity of the contact region as the solvent viscosity β. Beyond this point elasticity will not affect the spreading speed, as predicted by our simulation, where the variation of k from Wi = 45 to Wi = 450 is small.

However, the Oldyrod-B model does not account for molecule migration. The faster motion of contact line may rise from the fact that given the same contact line speed (Ca), the elastic interface is more bent than the Newtonian one [9,19], which results in a larger driving force that pulls the contact line harder.

The results of the shear-thinning Giesekus fluid are less comparable to the experimental data from literature because most studies on wetting of shear-thinning fluids used power-law fluids, which are rheologically different from the Giesekus fluid we present in this study. In fact, the shear-thinning xanthan gum is found not to follow the Tanner-Voinov-Hoffman relation [18]. The reason the Tanner-Voinov-Hoffman relation is valid for the Giesekus fluid may stem from the fact that the presented Giesekus model has very similar form as the Oldroyd-B model, except for the nonlinear term that sets the plateau of $\boldsymbol{\tau}_p$. In the late time dynamics, the contact area is of low shear rate, except for the contact point where the flow creates singularity. Thus we will still have high shear rate at the contact point, which lies at a distance ϵ away from the wall. Around this point the polymeric stress does not depend on Wi, as it has reached the plateau. We expect some future spreading experiments on Giesekus fluids will verify our conclusion.

V. CONCLUSION

We conducted simulations on droplet spreading of viscoelastic fluids, specifically, the Oldroyd-B fluid and the Giesekus fluid. We observed that viscoelastic droplets spread faster than the Newtonian droplets, given identical density and zero shear viscosity. The non-Newtonian effect takes place in the interfacial region near the contact line, and both shear thinning and elasticity can enhance contact line motion during droplet spreading; however, the contact speed is limited by the solvent viscosity. Shear thinning reduces viscous drag on the contact line, while the reason elasticity can speed up the contact line remains mysterious. The presented numerical model combining the phase field method and viscoelastic constitutive laws successfully predicts several spreading behaviors discovered by experiments, despite the fact that some physics, e.g., molecule migration, are missing in our model.

ACKNOWLEDGMENTS

Computer time offered by the Swedish National Infrastructure for Computing (SNIC) is gratefully acknowledged. Y.W. would also like to give thanks for support from the National Natural Science Foundation of China (Grant No. 51176065).

[1] L. H. Tanner, The spreading of silicone oil drops on horizontal surfaces, J. Phys. D: Appl. Phys. **12**, 1473 (1979).

[2] Richard L. Hoffman, A study of the advancing interface, I. Interface shape in liquid gas systems, J. Colloid Interface Sci. **50**, 228 (1975).

[3] O. V. Voinov, Hydrodynamics of wetting, Fluid Dyn. **11**, 714 (1976).

[4] R. G. Cox, The dynamics of the spreading of liquids on a solid surface, Part 1. Viscous flow, J. Fluid Mech. **168**, 169 (1986).

[5] Alain Carré and Florence Eustache, Spreading kinetics of shear-thinning fluids in wetting and dewetting modes, Langmuir **16**, 2936 (2000).

[6] Salima Rafaï, Daniel Bonn, and Arezki Boudaoud, Spreading of non-Newtonian fluids on hydrophilic surfaces, J. Fluid Mech. **513**, 77 (2004).

[7] Salima Rafaï and Daniel Bonn, Spreading of non-Newtonian fluids and surfactant solutions on solid surfaces, Physica A (Amsterdam, Neth.) **358**, 58 (2005).

[8] Y. Wei, E. Rame, L. M. Walker, and S. Garoff, Dynamic wetting with viscous Newtonian and non-Newtonian fluids, J. Phys.: Condens. Matter **21**, 464126 (2009).

[9] Y. Wei, G. K. Seevaratnam, S. Garoff, E. Ramé, and L. M. Walker, Dynamic wetting of Boger fluids, J. Colloid Interface Sci. **313**, 274 (2007).

[10] Jeongin Han and Chongyoup Kim, Spreading of Boger fluid on horizontal surface, J. Non-Newtonian Fluid Mech. **202**, 120 (2013).

[11] Lin Fang, Hua Hu, and Ronald G. Larson, DNA configurations and concentration in shearing flow near a glass surface in a microchannel, J. Rheology (1978-present) **49**, 127 (2005).

[12] Vance Bergeron, Daniel Bonn, Jean Yves Martin, and Louis Vovelle, Controlling droplet deposition with polymer additives, Nature (London) **405**, 772 (2000).

[13] Regan Crooks, Justin Cooper-White, and David V. Boger, The role of dynamic surface tension and elasticity on the dynamics of drop impact, Chem. Eng. Sci. **56**, 5575 (2001).

[14] Vance Bergeron, Designing intelligent fluids for controlling spray applications, C. R. Phys. **4**, 211 (2003).

[15] Denis Bartolo, Arezki Boudaoud, Grégoire Narcy, and Daniel Bonn, Dynamics of Non-Newtonian Droplets, Phys. Rev. Lett. **99**, 174502 (2007).

[16] M. I. Smith and V. Bertola, Effect of Polymer Additives on the Wetting of Impacting Droplets, Phys. Rev. Lett. **104**, 154502 (2010).

[17] V. Bertola, Dynamic wetting of dilute polymer solutions: The case of impacting droplets, Adv. Colloid Interface Sci. **193-194**, 1 (2013).

[18] G. K. Seevaratnam, Y. Suo, E. Rame, L. M. Walker, and S. Garoff, Dynamic wetting of shear thinning fluids, Phys. Fluids (1994-present) **19**, 012103 (2007).

[19] Pengtao Yue and James J. Feng, Phase-field simulations of dynamic wetting of viscoelastic fluids, J. Non-Newtonian Fluid Mech. **189-190**, 8 (2012).

[20] Sungjune Jung, Stephen D. Hoath, and Ian M. Hutchings, The role of viscoelasticity in drop impact and spreading for inkjet printing of polymer solution on a wettable surface, Microfluidics Nanofluidics **14**, 163 (2012).

[21] John W. Cahn and John E. Hilliard, Free energy of a nonuniform system, I. Interfacial free energy, J. Chem. Phys. **28**, 258 (1958).

[22] David Jacqmin, Contact-line dynamics of a diffuse fluid interface, J. Fluid Mech. **402**, 57 (2000).

[23] Walter Villanueva and Gustav Amberg, Some generic capillary-driven flows, Int. J. Multiphase Flow **32**, 1072 (2006).

[24] D. M. Anderson, Geoffrey B. McFadden, and A. A. Wheeler, Diffuse-interface methods in fluid mechanics, Annu. Rev. Fluid Mech. **30**, 139 (1998).

[25] Robert Byron Bird, Robert Calvin Armstrong, and Ole Hassager, *Dynamics of Polymeric Liquids* (Wiley, New York, 1987), 2nd ed., Vol. 1: Fluid Mechanics.

[26] Pengtao Yue, Chunfeng Zhou, and James J. Feng, Sharp-interface limit of the Cahn-Hilliard model for moving contact lines, J. Fluid Mech. **645**, 279 (2010).

[27] Patrick R. Amestoy, Iain S. Duff, and J-Y. L'Excellent, Multifrontal parallel distributed symmetric and unsymmetric solvers, Comput. Methods Appl. Mech. Eng. **184**, 501 (2000).

[28] Patrick R. Amestoy, Iain S. Duff, Jean-Yves L'Excellent, and Jacko Koster, A fully asynchronous multifrontal solver using distributed dynamic scheduling, SIAM J. Matrix Anal. & Appl. **23**, 15 (2001).

[29] Alice W. Liu, David E. Bornside, Robert C. Armstrong, and Robert A. Brown, Viscoelastic flow of polymer solutions around a periodic, linear array of cylinders: Comparisons of predictions for microstructure and flow fields, J. Non-Newtonian Fluid Mech. **77**, 153 (1998).

[30] Gustav Amberg, Robert Tönhardt, and Christian Winkler, Finite element simulations using symbolic computing, Math. Comput. Simul. **49**, 257 (1999).

[31] Andreas Carlson, Minh Do-Quang, and Gustav Amberg, Dissipation in rapid dynamic wetting, J. Fluid Mech. **682**, 213 (2011).

[32] Antonin Eddi, Koen G. Winkels, and Jacco H. Snoeijer, Short time dynamics of viscous drop spreading, Phys. Fluids (1994-present) **25**, 013102 (2013).

[33] Daniel Bonn, Jens Eggers, Joseph Indekeu, Jacques Meunier, and Etienne Rolley, Wetting and spreading, Rev. Mod. Phys. **81**, 739 (2009).

[34] E. B. Dussan V, Enrique Ramé, and Stephen Garoff, On identifying the appropriate boundary conditions at a moving contact line: An experimental investigation, J. Fluid Mech. **230**, 97 (1991).

[35] B. Yesilata, Christian Clasen, and Gareth H. McKinley, Nonlinear shear and extensional flow dynamics of wormlike surfactant solutions, J. Non-Newtonian Fluid Mech. **133**, 73 (2006).

[36] Hongbo Ma and Michael D. Graham, Theory of shear-induced migration in dilute polymer solutions near solid boundaries, Phys. Fluids (1994-present) **17**, 083103 (2005).